San Francisco Bay Area Portable Seismograph Deployments

In a series of recent papers (Frankel et al., 2001; Hartzell et al., 2003; Hartzell et al., 2006; Harmsen et al., 2008; Hartzell et al., 2010; 2014) the Santa Clara Valley and the greater San Francisco Bay Area have served as a laboratory for the investigation of site response and wave propagation effects. These study areas are representative of geologic features found in other urbanized sedimentary basins around the world, and have significance for ground motion estimation beyond their locations in the northern California Bay Area. By understanding the underlying structural features responsible for the observed variations in ground motion at these sites, we are better equipped to transplant that knowledge to other seismically at-risk sedimentary basins. Some of the wave propagation phenomenon that we investigate include: 1) surface wave generation and reflection at the edges of a sedimentary basin and propagation within the basin, 2) trapping of energy by younger basins within valley fill, 3) topographic and variable attenuation effects at the basin margins, and 4) fault guided waves and amplification of ground motion in low velocity fault zones. A better understanding of the propagation and amplification of seismic waves in sedimentary basins requires an appreciation of varied structural influences, several of which may be at work at a single site. We select sites for study because they present different aspects of ground motion that are related to the underlying geologic structure, that is, the shape and depth of a basin or the topography and competency of the rock. Relating the importance of geologic structures to aspects of wave propagation has been the subject of considerable previous study and continues to be of significant interest in seismic hazard evaluation (Li et al., 1994; Hatayama et al., 1995; Field, 1996; Kawase, 1996; Graves et al., 1998; Joyner, 2000; Rovelli et al., 2001; Spudich and Olsen, 2001; Adams et al., 2003; Cornou et al., 2003a; 2003b; Williams et al., 2005; Wang et al., 2006; Frankel et al., 2009; Lee et al., 2009b; among others). We use a variety of ground motion analysis and simulation techniques as required by our investigations of the ground motion. These methods include: 1) spectral ratios, 2) *f-k* array analysis, 3) 2D and 3D numerical wave propagation simulations, and 4) a full-waveform 1D structure inversion method. The variety of our modeling and investigative tools reflects the complexity of the ground motion and the diversity of wave propagation phenomena present in sedimentary basins.

Background on Previous Basin Studies in the Study Area

Studies in the Santa Clara Valley include Frankel et al. (1991) and Frankel and Vidale (1992), who concluded that observed long-duration velocity and displacement waveforms are composed of mainly surface waves formed at the edges of the basin. Hartzell et al. (2001) found a complicated pattern of site response in the town of Los Gatos on the southwestern margin of the valley, attributed to variable thickness of soft sediments formed by crosscutting thrust faults. Fletcher et al. (2003) utilized records of local earthquakes to investigate basin structure and site response. They found greater travel time delays and increased longer-period amplification factors over the Cupertino and Evergreen Cenozoic basins, previously identified in gravity data (Brocher et al., 1997; Roberts et al., 2004) within the Santa Clara Valley. Dolenc et al. (2005) and Dolenc and Dreger (2005) compared P-wave travel times and microseism horizontal to vertical spectral ratios from the Fletcher et al. (2003) instrument deployment with predictions of two Bay Area velocity models (USGS, Brocher et al. (1997) and Jachens et al. (1997); and UC Berkeley, Stidham et al. (1999)) and found a strong correlation with basin depth.

The introduction of our San Jose portable seismic array of approximately 50 instruments in 1999 greatly expanded the database of ground motion observations in the Santa Clara Valley (Figure 1). Utilizing the initial station deployment over the Evergreen Basin on the northeastern side of the valley, Frankel et al. (2001) found that shear-wave site amplification increased further from the edge of the valley with the largest values above the southwestern edge of the Evergreen Basin. Array analysis also revealed late-arriving surface waves originating at the southern end of the Santa Clara Valley for regional sources to the east. Hartzell et al. (2003), using this same station configuration, showed that site response spectra could be inverted to yield shallow shear-wave velocity profiles down to a few hundred meters. In addition, ground motion from regional events produced larger site amplification factors than local earthquakes, at frequencies below 3Hz, due to stronger surface-wave generation. In 2004 the array was reconfigured to include stations stretching across the width of the valley and over the Cupertino Basin on the southwestern side (Figure 2, new station locations in red and previous station locations in black). Hartzell et al. (2006) used 2D finite difference to model the observed shift in maximum shear-wave amplification over the southwestern edge of the Evergreen Basin. They also showed that

the Cupertino Basin has a significantly lower site response than the Evergreen Basin. In 2006 the array was again reconfigured to investigate other aspects of site response, including a line across the Hayward fault on the northeastern side of the valley and an array climbing out of the valley onto the hills on the southwestern side (Figure 3). The change in 2008 removed the array over the Cupertino Basin and moved these stations to the San Leandro and Livermore Basins on the east side of the San Francisco Bay. Analysis of ground motion records from the San Leandro sites shows significant surface wave development in the thickening sediments to the west of the Hayward fault (Frankel and Carver, 2009). Most recently in 2013 our instrumentation was redeployed to form the Tri-Valley array of 32 stations consisting of three lines of stations across the communities of San Ramon/Dublin, Pleasanton, and Livermore (Figure 4). This new array is designed to track the formation and propagation of surface waves across the Livermore Valley as well as study the influence of basin depth on site response.

Parallel to the above studies, a 3D velocity model of the region has been developed and evaluated against observed travel times and waveforms. This model is based on the geologic model of Jachens et al. (2001; 2005), which has gone through successive refinements and improvements to the seismic velocities (Brocher et al., 1997; 2005; 2006). Simulations of ground motion in the region using 3D velocity models have been done by Frankel and Vidale (1992), Larsen et al. (1997), Stidham et al. (1999), Dreger et al. (2001), Hartzell et al. (2006), Harmsen et al. (2008), Aagaard et al. (2008a, 2008b), and Rodgers et al. (2008). These studies have been useful for evaluating and adjusting the gross seismic velocities of geologic units within the 3D model.

Some Results of Our Basin Studies

We have analyzed ground motion records from several directed studies in the Santa Clara Valley and the greater San Francisco Bay Area to investigate variations in site response and wave propagation effects that could be common to other urban sedimentary basins. Important differences in ground motion are shown to exist over length scales from a few hundred meters to a few kilometers, that are related to shallow crustal features of the basin or its margins. Our studies have also demonstrated that different wave propagation phenomena can occur in different

areas of a single sediment-filled valley that lead to the observed complexity of ground motion. By covering a number of important structural influences, our studies give an appreciation of the range of effects that should be considered in seismic hazard assessment in sedimentary basins.

An array of stations placed over the edge of the Santa Clara Valley (Blossom Hill) and extending from the young alluvial fill in the valley to Miocene rock on a 100m high ridge shows significant differences in ground motion above 1Hz. Site amplification in the frequency band 2 to 4Hz is 2.5 times greater on the ridge than in the valley. High frequency velocity records (lowpassed at 15Hz) from local earthquakes can have average amplitudes 5 times higher on the ridge. 3D finite-element modeling was employed to investigate the importance of topography, attenuation, and local fault zone complexity. Although significant differences in amplitudes are seen comparing synthetics with and without attenuation, the observed velocity ratios required the addition of a low-velocity zone along the Shannon-Berrocal fault zone. A prominent basin-edge effect is seen in the synthetics and to a lesser extent in the data. The smaller amplitude basin-edge induced waves in the data records may be due to the complexity of the ridge/basin contact.

Cenozoic basins in the San Francisco Bay area play a major role in shaping the ground motion in a sediment-filled valley. Two such basins in the Santa Clara Valley, the Cupertino and Evergreen, have markedly different responses that can be attributed to their differences in age, structure, and basin fill. Over the instrumented portion of the Cupertino Basin the ground motion response is moderate in amplitude and very uniform. This character of the ground motion is attributed to the nearly flat basement contact and the flat-lying sediments of the basement fill. In contrast, ground motion over the Evergreen Basin is about 75% larger. The pattern of shear-wave site amplification is asymmetric, peaking near the southwestern edge of the Evergreen Basin, whereas the maximum in vertical amplification is coincident with the deepest part of the basin. These observations can be attributed to: 1) an assumed younger age for the Evergreen Basin and thus lower velocities for the basin fill compared to the Cupertino Basin, 2) the observed decrease in shallow shear-wave velocities moving away from the edge of the valley toward the southwestern edge of the Evergreen Basin, and 3) the fault-controlled, steeply-dipping southwestern boundary of the Evergreen Basin and its V shaped cross section. In addition, we have shown that a long, narrow basin, like the Evergreen, is sensitive to the direction of approach

of seismic waves. Seismic energy traveling along the long axis of a basin is more efficiently trapped within the basin compared to waves impinging at near right-angles to the long axis.

Plane wave analysis reveals the importance of surface waves in basin ground motion, and their reflection/formation at basin edges and other discontinuities in seismic properties. A basin-edge surface wave is captured forming at the southwestern edge of the Santa Clara Valley at the base of Blossom Hill. Sources in line with the northwest/southeast elongation of the Santa Clara Valley appear to favor surface wave propagation up and down the length of the valley. For sources located outside the Santa Clara Valley, such as on the southern Calaveras fault, surface waves are generated during wave propagation across the valley. Then, surface waves are clearly seen traveling in the opposite direction, either created by body-wave conversions in the shallowing sediments near the edge of the basin or reflected from the basin margin. In addition, surface waves appear to be reflected from a 200m offset in the basement at the Hayward fault. Similar phenomena were observed by Hartzell et al. (2003), who reported surface waves apparently reflected from the sharp, fault-controlled southwestern edge of the Evergreen Basin.

As has been observed for other faults in California, such as the Landers (Li et al., 1994; 2007; Peng et al., 2003), Calaveras (Cormier and Spudich, 1984; Spudich and Olsen, 2001), and San Jacinto (Li et al., 1997a), the Hayward fault is shown to have a low-velocity fault zone, originating from a region of fractured rock. This zone is estimated to be 100 to 200m wide from an interpreted fault zone guided wave. The low-velocity fault zone leads to amplification of seismic waves above 1Hz and contributes to increased seismic hazard along the trace of the fault in addition to the hazard from fault rupture. A nonlinear, global search-based inversion of the waveforms across the Hayward fault is shown to be a useful tool in imaging near-surface seismic velocities.

Background to Topographic Effects Studies

Topography has long been known to modify observed surface ground motions. Sato (1955) considered the superposition of plane waves to investigate reflected waves from a corrugated free surface. Aki and Larner (1970) introduced a frequency domain method to study irregularly

shaped interfaces imbedded in a half-space. Large recorded motions from the 1971 San Fernando, CA, earthquake, particularly at the Pacoima Dam site, stimulated interest in the effects of topography. Bouchon (1973) applying an extension of the Aki and Larner (1970) method and Boore (1972) using finite difference, both considered simple 2D topography and concluded that significant amplification occurs at topographic highs for incident wavelengths comparable to the width of the topographic feature. Correspondingly, deamplification occurs at topographic depressions. Bard (1982) further considered the effects of incident wave type, frequency, incidence angle, and anomaly height. Systematically greater amplification was found for incident S-waves than P-waves. Amplification was also shown to increase with increasing slope of the topographic high and decreasing angle of incidence. Geli *et al.* (1988) provided a useful summary of theoretical and observed amplification values as well as additional calculations for 2D structures with subsurface layering and neighboring topographic features. Their crest-to-base spectral amplification values range up to a factor of 10 or more. Amplification at the crest of topography was shown to be a maximum for a frequency of c/l, where c is the material velocity and l is the base width of the topographic feature. The compilation of available data showed that numerical simulations often underestimate observed amplification, which was related to the difficulty of isolating topographic effects from other site effects and the two-dimensionality often assumed in the numerical calculations. Sanchez-Sesma and Campillo (1991) developed a boundary integral method and simulated topographic effects for a variety of hypothetical features in a half-space. They found relative amplifications that can be greater than 10 due to complicated patterns of amplification and deamplification, but that absolute levels of amplification were generally lower than about four times the amplitude of the incoming wave. They stressed the large variability of spectral content of ground motion in both frequency and space. Bouchon *et al.* (1996) developed a semi-analytical semi-numerical method to calculate the diffraction of seismic waves by three-dimensional topography of arbitrary shape. Since then fully numerical finite-element methods have dominated the simulation of topographic effects in 3D media. Ma *et al.* (2007) showed that mountains produce a shielding effect by the scattering of predominantly surface waves, resulting in lower ground motions in the region beyond the topography. Lee *et al.* (2009a, b) found that topography can change peak ground velocity (PGV) in mountainous areas by ±50% compared to a half space and the relative change in peak ground acceleration (PGA) between a valley and a ridge can be as high as a factor of 2. Shaking was also found to be

strongly dependent on the scale of the topographic features in relation to the wavelength of the source content.

These theoretical investigations have been complemented by the analysis of recorded motions over topographic features. Davis and West (1973) calculated crest-to-base ratios in the time and frequency domains for three mountains in southern California and Nevada using aftershocks of the 1971 San Fernando earthquake and a cavity collapse following a Nevada Test Site (NTS) detonation. In general the wavelengths corresponding to the maximum amplifications are comparable to the mountain widths, consistent with theory, but the observed amplifications are much larger. Rogers *et al.* (1974) considered only time-domain crest-to-base amplitude ratios for another NTS explosion. Their observed amplitude ratios were consistent with theory, perhaps aided by the simple geometry of the topography and source alignment. Griffiths and Bollinger (1979) also only used time-domain crest-to-base amplitude ratios across the approximately 2D topography of the Appalachian Mountains and sources from mainly quarry and mine blasts. They observed a large scatter in values with an average amplification significantly larger than theoretical predictions. Pedersen *et al.* (1994) obtained general agreement between observations and simulations for amplification over a simple ridge in Greece. They conclude that topographic deamplification at a reference site can lead to over-estimation of ridge-crest amplification compared to theoretical predictions. Studies of aftershocks of the 1994 Northridge, CA, earthquake on a hill in Tarzana, prompted by large mainshock ground motions, pointed out the directional seismic response of the hill that results in a strong amplification of ground motion transverse to the direction of elongation of the hill (Spudich *et al.*, 1996; Bouchon and Barker, 1996). Massa *et al.* (2010) instrumented a ridge in central Italy and calculated horizontal-to-vertical-component spectral ratios (HVSR) and the ridge-crest-to-base spectral ratios for small local earthquakes. Results from the reference site crest-to-base spectral ratios were considered to be more accurate. Amplification factors increased when the direction of ground motion was perpendicular to the ridge elongation. Panzera *et al.* (2011) advocated the use of HVSR using ambient noise sources to study topographic effects on a raised peninsula on Sicily. They found HVSR desirable because it avoided the difficulty of finding a reference site free of topographic effects. They showed a consistency between HVSR analysis and polarization analysis in the directional effect having an azimuth transverse to the major axis of the peninsula.

Despite these studies there are still lingering questions about the reliability of theoretical calculations in the evaluation of topographic effects and the appropriateness of earthquake versus ambient noise sources and the types of data analysis. In our work we combine analysis of ground motion recordings from field studies in a mountainous regions of the San Francisco Bay Area, CA, with full 3D finite-element simulations using an accurate 10 m digital elevation model (DEM). Although data and theory have been compared in several previous investigations, as referenced above, earlier studies have mostly used simplistic 2D models to represent complicated real-world conditions. In the analysis of the ground motion records we compare reference-site-based spectral ratios with HVSR for local earthquake sources. We also compute HVSR from ambient noise and investigate the directionality characteristics of the site amplification.

Station Deployments for Study of Topographic Effects

A previous field deployment consisted of eight stations in two separate lines of four stations each, straddling Poverty Ridge in the Diablo Mountains east of San Jose, CA (Hartzell et al., 2014) (Figure 5). Our current topographic deployment consists of eight stations in a single line across Mission Peak just north of the Poverty Ridge area (Figure 6, 7, 8, 9, and 10). These locations were selected for our investigation of topographic effects for three reasons: 1) their proximity to the Calaveras fault, which is the source of numerous small earthquakes, 2) the approximate linear trend of the ridges, and 3) the significant topographic relief. Instrumentation includes Compact Trillium seismometers and RefTek recorders. The sensors were buried in a small vault approximately 20 cm below the ground surface. In both cases deployment is for one year.

Because of the recognized difficulty of distinguishing topographic effects from other site effects resulting from soft surficial deposits, a mention of the local setting of each instrument is appropriate for our interpretation of the data. Poverty Ridge is composed of Franciscan Complex metamorphic rocks of Cretaceous age. Each sensor, except the two ridge crest sites, was placed in contact with a rock outcrop or within approximately two meters of a rock outcrop on fractured material from the same unit. Hard rock is not visible in the immediate vicinity of the ridge crest sites because of the development of a soil layer. However, rock is seen in road cuts at an

elevation of a few meters below the top of the ridge. Most of our observations lie below a frequency of 3 Hz. For a spectral peak at 3 Hz to have its origin from a shallow resonance would require a sediment thickness of 25 m for a shear wave velocity of 300 m/s. The general absence of thick sediments at the station locations makes it possible to identify the uncontaminated topographic effects. This argument is bolstered by our synthetic modeling results that fit the observations well without the effects of any near-surface layering.

Some Results of Our Topographic Effects Studies

Previous studies of topographic effects have shown a general pattern of under prediction of amplification factors from theoretical calculations compared with the amplification seen in data records. Our results, detailed in Hartzell et al. (2014), show that the amplitude of the fundamental resonance peak can be well predicted using an accurate 3D digital elevation model and velocity model. However, this conclusion needs to be tempered with the fact that ground motion on topography is sensitive to the direction of approach and polarization of the incoming waves, particularly at frequencies above the fundamental resonance. Although there is an indication of the same spectral peaks above the fundamental resonance in the theoretical spectra as in the observed spectra for sources approximately in line with the major axis of the ridge, the amplitude of these peaks were under predicted. Our results support the use of topography in ground motion simulations to obtain more accurate predictions of earthquake ground motions up through the fundamental resonance frequency of the topographic feature.

Poverty Ridge shows a ridge-crest amplification of a factor of 3 to 4 at the fundamental resonance of approximately 0.5 to 1.0 Hz relative to a ridge-base site. The frequency of the fundamental resonance can shift with the azimuth and angle of incidence of the incoming waves, probably as a result of a more favorable resonance over a different ridge dimension. Reference site spectral ratios are found to be the most robust at defining the amplitude of the fundamental resonance as well as the frequency and amplitude of higher-frequency resonances. Horizontal-to-Vertical-Spectral-Ratio (HVSR) analysis of earthquake records usually recovers the frequency and amplitude of the fundamental resonance, but does not show higher frequency peaks, possibly due to increased scattered wave energy on the vertical component. Ambient noise is found to be a poor source for the study of topographic effects. Spectral ratios over topography from ambient

noise are broad functions of frequency with lower amplitude than spectra from earthquakes. These observations are probably due to the dominance of surface waves in ambient noise as contrasted with body waves in local earthquake records and the averaging over azimuth of ambient noise sources. Strong directionality is seen in the topographic resonance frequencies that are transverse to the major axes of the topographic features.

Basin Effects References

Aagaard, B. T., T. M. Brocher, D. Dolenc, D. Dreger, R. W. Graves, S. Harmsen, S. Hartzell, S. Larsen, and M. L. Zoback (2008a). Ground-motion modeling of the 1906 San Francisco earthquake, Part I: Validation using the 1989 Loma Prieta earthquake, *Bull. Seism. Soc. Am.* **98**, 989-1011.

Aagaard, B. T., T. M. Brocher, D. Dolenc, D. Dreger, R. W. Graves, S. Harmsen, S. Hartzell, S. Larsen, K. McCandless, S. Nilsson, N. Anders Petersson, A. Rodgers, B. Sjogreen, and M. L. Zoback (2008b). Ground-motion modeling of the 1906 San Francisco earthquake, Part II: Ground-motion estimates for the 1906 earthquake and scenario events, *Bull. Seism. Soc. Am.* **98**, 1012-1046.

Adams, B. M., N. M. Osborne, and J. J. Taber (2003). The basin-edge effect from weak ground motions across the fault-bounded edge of the lower Hutt Valley, New Zealand, *Bull. Seism. Soc. Am.* **93**, 2703-2716.

Brocher, T., E. Brabb, R. Catchings, G. Fuis, T. Fumal, R. Jachens, A. Jayko, R. Kayen, R. McLaughlin, T. Parsons, M. Rymer, R. Stanley, and C. Wentworth (1997). A crustal-scale 3D seismic velocity model for the San Francisco Bay area, California, *EOS Trans. AGU* **78**, F435.

Brocher, T. M., R. C. Jachens, R. W. Graymer, C. M. Wentworth, B. Aagaard, and R. W. Simpson (2005). A new community 3D seismic velocity model for the San Francisco Bay area:

USGS Bay Area velocity model 05.0.0 (abstract), Southern California Earthquake Center annual meeting.

Brocher, T., B. Aagaard, R. Simpson, and R. Jachens (2006). The new USGS 3D seismic velocity model for Northern California (abstract), *Seism. Res. Lett.* **77**, 271.

Cormier, V. F., and P. Spudich (1984). Amplification of ground motion and waveform complexity in fault zones: examples from the San Andreas and Calaveras faults, *Geophys. J. R. astr. Soc.* **79**, 135-152.

Cornou, C., P.-Y. Bard, and M. Dietrich (2003a). Contribution of dense array analysis to the identification and quantification of basin-edge-induced waves, part I: methodology, *Bull. Seism. Soc. Am.* **93**, 2604-2623.

Cornou, C., P.-Y. Bard, and M. Dietrich (2003b). Contribution of dense array analysis to the identification and quantification of basin-edge-induced waves, part II: application to Grenoble Basin (French Alps), *Bull. Seism. Soc. Am.* **93**, 2624-2648.

Dolenc, D., and D. Dreger (2005). Microseismic observations in the Santa Clara Valley, California, *Bull. Seism. Soc. Am.* **95**, 1137-1149.

Dolenc, D., D. Dreger, and S. Larsen (2005). Basin structure influences on the propagation of teleseismic waves in the Santa Clara Valley, California, *Bull. Seism. Soc. Am.* **95**, 1120-1136.

Dreger, D., D. Dolence, C. Stidham, L. Baise, and S. Larsen (2001). Evaluating 3D Earth models for the purpose of strong ground motion simulation, *Seism. Res. Lett.* **72**, no. 2, 278.

Field, E. H. (1996). Spectral amplification in a sediment-filled valley exhibiting clear basin-edge-induced waves, *Bull. Seism. Soc. Am.* **86**, 991-1005.

Fletcher, J. B., J. Boatwright, and A. G. Lindh (2003). Wave propagation and site response in the Santa Clara Valley, *Bull. Seism. Soc. Am.* **93**, 480-500.

Frankel, A., S. Hough, P. Friberg, and R. Busby (1991). Observations of Loma Prieta aftershocks from a dense array in Sunnyvale, California, *Bull. Seism. Soc. Am.* **81**, 1900-1922.

Frankel, A., and J. Vidale (1992). A three-dimensional simulation of seismic waves in the Santa Clara Valley, California, from a Loma Prieta aftershock, *Bull. Seism. Soc. Am.* **82**, 2045-2074.

Frankel, A., D. Carver, E. Cranswick, T. Bice, R. Sell, and S. Hanson (2001). Observations of basin ground motions from a dense seismic array in San Jose, California, *Bull. Seism. Soc. Am.* **91**, 1-12.

Frankel, A., and D. Carver (2009). Basin surface waves and ground-motion amplification in the San Leandro and Livermore Basins, California: Implications for seismic hazard, *Seism. Res. Lett.* **80**, no. 2.

Frankel, A., W. Stephenson, and D. Carver (2009). Sedimentary basin effects in Seattle, Washington: ground-motion observations and 3D simulations, *Bull. Seism. Soc. Am.* **99**, 1579-1611.

Graves, R. W., A. Pitarka, and P. G. Somerville (1998). Ground-motion amplification in the Santa Monica area: effects of shallow basin-edge structure, *Bull. Seism. Soc. Am.* **88**, 1224-1242.

Harmsen, S., S. Hartzell, and Pengcheng Liu (2008). Simulated ground motion in the Santa Clara Valley, California, and vicinity from **M** $\geq$ 6.7 scenario earthquake, *Bull. Seism. Soc. Am.* **98**, 1243-1271.

Hartzell, S., D. Carver, and R. A. Williams (2001). Site response, shallow shear-wave velocity, and damage in Los Gatos, California, from the 1989 Loma Prieta earthquake, *Bull. Seism. Soc. Am.* **91**, 468-478.

Hartzell, S., D. Carver, R. A. Williams, S. Harmsen, and A. Zerva (2003). Site response, shallow shear-wave velocity, and wave propagation at the San Jose, California, dense seismic array, *Bull. Seism. Soc. Am.* **93**, 443- 464.

Hartzell, S., S. Harmsen, R. A. Williams, D. Carver, A. Frankel, G. Choy, Pengcheng Liu, R. C. Jachens, T. M. Brocher, and C. M. Wentworth (2006). Modeling and validation of a 3D velocity structure for the Santa Clara Valley, California, for seismic-wave simulations, *Bull. Seism. Soc. Am.* **96**, 1851-1881.

Hartzell, S., L. Ramirez-Guzman, D. Carver, and P.-C. Liu (2010). Short baseline variations in site response and wave-propagation effects and their structural causes: Four examples in and around the Santa Clara Valley, California, *Bull. Seism. Soc. Am.* **100**, 2264-2286.

Hartzell, S., M. Meremonte, L. Ramirez-Guzman, and D. McNamara (2014). Ground motion in the presence of complex topography: Earthquake and ambient noise sources, *Bull. Seism. Soc. Am.* **104**, doi: 10.1785/0120130088.

Hatayama, K., K. Matsunami, I. Tomotaka, and K. Irikura (1995). Basin-induced Love waves in the eastern part of the Osaka Basin, *J. Phys. Earth* **43**, 131-155.

Jachens, R. C., R. F. Sikora, E. E. Brabb, C. M. Wentworth, T. M. Brocher, M. S. Marlow, and C. W. Roberts (1997). The basement interface: San Francisco Bay area, California, 3-D seismic velocity model, *EOS Trans. AGU* **78**, F436.

Jachens, R. C., C. M. Wentworth, D. L. Gautier, and S. Pack (2001). 3D geologic maps and visualization: A new approach to the geology of the Santa Clara (Silicon) Valley, California, *U.S. Geol. Surv. Open-File Rept. 01-223.*

Jachens, R. C., C. M. Wentworth, R. W. Simpson, R. W. Graymer, S. E. Graham, R. A. Williams, R. J. McLaughlin, and V. E. Langenheim (2005). Three-dimensional geologic map of the Santa Clara Valley and adjacent uplands, California, Geol. Soc. Am., Cordilleran Section, 101st Annual Meeting, 29 April-1 May 2005, *GSA Abstracts with Programs* **37**, no. 4, 89.

Joyner, W. B. (2000). Strong motion from surface waves in deep sedimentary basins, *Bull. Seism. Soc. Am.* **90**, v. 6B, S95-S112.

Kawase, H. (1996). The cause of the damage belt in Kobe: "The basin-edge effect", constructive interference of the direct S-wave with basin induced diffracted/Rayleigh waves, *Seism. Res. Lett.* **67**, 25-34.

Larsen, S., M. Antolik, D. Dreger, C. Stidham, C. Schultz, A. Lomax, and B. Romanowicz (1997). 3D models of seismic wave propagation; simulating scenario earthquakes along the Hayward Fault, *Seism. Res. Lett.* **68**, no. 2, 328.

Lee, Shiann-Jong, Yu-Chang Chan, D. Komatitsch, Bor-Shouh Huang, and J. Tromp (2009b). Effects of realistic surface topography on seismic ground motion in the Yangminshan region of Taiwan based upon the spectral-element method and LiDAR DTM, *Bull. Seism. Soc. Am.* **99**, 681-693.

Li, Yong-Gang, K. Aki, D. Adams, A. Hasemi, and W. L. Lee (1994). Seismic guided waves trapped in the fault zone of the Landers, California, earthquake of 1992, *J. Geophys. Res.* **99**, 11705-11722.

Li, Yong-Gang, K. Aki, and F. L. Vernon (1997a). San Jacinto fault zone guided waves: a discrimination for recently active fault strands near Anza, California, *J. Geophys. Res.* **102**, 11689-11701.

Li, Hongyi, L. Zhu, and H. Yang (2007). High-resolution structures of the Landers fault zone inferred from aftershock waveform data, *Geophys. J. Int.*, doi: 10.1111/j.1365-246X.2007.03608.x

Peng, Z., Y. Ben-Zion, A. J. Michael, and L. Zhu (2003). Quantitative analysis of seismic fault zone waves in the rupture zone of the 1992 Landers, California, earthquake: evidence for a shallow trapping structure, *Geophys. J. Int.* **155**, 1021-1041.

Roberts, C. W., R. C. Jachens, D. A. Ponce, and V. E. Langenheim (2004). Isostatic residual gravity map of the Santa Clara Valley and vicinity, California, *U.S. Geol. Surv. Open-File Rept. 04-1297.*

Rodgers, A., N. Anders Petersson, S. Nilsson, B. Sjogreen, and K. McCandless (2008). Broadband waveform modeling of moderate earthquakes in the San Francisco Bay area and preliminary assessment of the USGS 3D seismic velocity model, *Bull. Seism. Soc. Am.* **98**, 969-988.

Rovelli, A., L. Scognamiglio, F. Marra, and A. Caserta (2001). Edge-diffracted 1-sec surface waves observed in a small-size intramountain basin (Colfiorito, central Italy), *Bull. Seism. Soc. Am.* **91**, 1851-1866.

Spudich, P., and K. B. Olsen (2001). Fault zone amplified waves as a possible seismic hazard along the Calaveras fault in central California, *Geophys. Res. Lett.* **28**, 2533-2536.

Stidham, C., D. Dreger, M. Antolik, S. Larsen, and B. Romanowicz (1999). Three-dimensional structure influences on the strong motion wavefield of the 1989 Loma Prieta earthquake, *Bull. Seism. Soc. Am.* **89**, 1184-1202.

Wang, G.-Q., G.-Q. Tang, D. M. Boore, G. Van Ness Burbach, C. R. Jackson, X.-Y. Zhou, and Q.-L. Lin (2006). Surface waves in the western Taiwan coastal plain from an aftershock of the 1999 Chi-Chi, Taiwan, earthquake, *Bull. Seism. Soc. Am.* **96**, 821-845.

Williams, R. A., R. W. Simpson, R. C. Jachens, W. J. Stephenson, J. K. Odum, and D. A. Ponce (2005). Seismic reflection evidence for a northeast-dipping Hayward fault near Fremont, California: implications for seismic hazard, *Geophys. Res. Lett.* **32**, L13301.

Topographic Effects References

Aki, K., and K. L. Larner (1970). Surface motion of a layered medium having an irregular interface due to incident plane SH waves, *J. Geophys. Res.* **75**, 933-954.

Bard, P.-Y. (1982). Diffracted waves and displacement field over two-dimensional elevated topographies, *Geophys. J. R. Astr. Soc.* **71**, 731-760.

Boore, D. M. (1972). A note on the effect of simple topography on seismic SH waves, *Bull. Seism. Soc. Am.* **62**, 275-284.

Bouchon, M. (1973). Effect of topography on surface motion, *Bull. Seism. Soc. Am.* **63**, 615-632.

Bouchon, M., and J. S. Barker (1996). Seismic response of a hill: The example of Tarzana, California, *Bull. Seism. Soc. Am.* **86**, 66-72.

Bouchon, M., C. A. Schultz, and M. N. Toksoz (1996). Effect of three-dimensional topography on seismic motion, *J. Geophys. Res.* **101**, 5835-5846.

Davis, L. L., and L. R. West (1973). Observed effects of topography on ground motion, *Bull. Seism. Soc. Am.* **63**, 283-298.

Geli, L., P.-Y. Bard, and B. Jullien (1988). The effect of topography on earthquake ground motion: A review and new results, *Bull. Seism. Soc. Am.* **78**, 42-63.

Griffiths, D. W., and G. A. Bollinger (1979). The effect of Appalachian mountain topography on seismic waves, *Bull. Seism. Soc. Am.* **69**, 1081-1105.

Hartzell, S., M. Meremonte, L. Ramirez-Guzman, and D. McNamara (2014). Ground motion in the presence of complex topography: Earthquake and ambient noise sources, *Bull. Seism. Soc. Am.* **104**, doi: 10.1785/0120130088.

Lee, S.-J., D. Komatitsch, B.-S. Huang, and J. Tromp (2009a). Effects of topography on seismic-wave propagation: An example from northern Taiwan, *Bull. Seism. Soc. Am.* **99**, 314-325.

Lee, S.-J., Y.-C. Chan, D. Komatitsch, B.-S. Huang, and J. Tromp (2009b). Effects of realistic surface topography on seismic ground motion in the Yangminshan region of Taiwan based upon the spectral-element method and LiDAR DTM, *Bull. Seims. Soc. Am.* **99**, 681-693.

Ma, S., R. J. Archuleta, and M. T. Page (2007). Effects of large-scale surface topography on ground motions, as demonstrated by a study of the San Gabriel Mountains, Los Angeles, California, *Bull. Seism. Soc. Am.* **97**, 2066-2079.

Massa, M., S. Lovati, E. D'Alema, G. Ferretti, and M. Bakavoli (2010). An experimental approach for estimating seismic amplification effects at the top of a ridge, and the implication for ground-motion predictions: The case of Narni, Central Italy, *Bull. Seism. Soc. Am.* **100**, 3020-3034.

Panzera, F., G. Lombardo, and R. Rigano (2011). Evidence of topographic effects through the analysis of ambient noise measurements, *Seism. Res. Lett.* **82**, 413-419.

Pedersen, H., B. Le Brun, D. Hatzfeld, M. Campillo, and P.-Y. Bard (1994). Ground-motion amplitude across ridges, *Bull. Seism. Soc. Am.* **84**, 1786-1800.

Rogers, A. M., L. J. Katz, and T. J. Bennett (1974). Topographic effects on ground motion for incident P waves: A model study, *Bull. Seism. Soc. Am.* **64**, 437-456.

Sanchez-Sesma, F. J., and M. Campillo (1991). Diffraction of P, SV, and Rayleigh waves by topographic features: A boundary integral formulation, *Bull. Seism. Soc. Am.* **81**, 2234-2253.

Sato, R. (1955). Reflection of elastic waves at a corrugated free surface (in Japanese), *J. Seism. Soc. Japan, Ser. 2*, **8**, 121.

Spudich, P., M. Hellweg, and W. H. K. Lee (1996). Directional topographic site response at Tarzana observed in aftershock of the 1994 Northridge, California, earthquake: Implications for mainshock motions, *Bull. Seism. Soc. Am.* **86**, S193-S208.

Figure 1

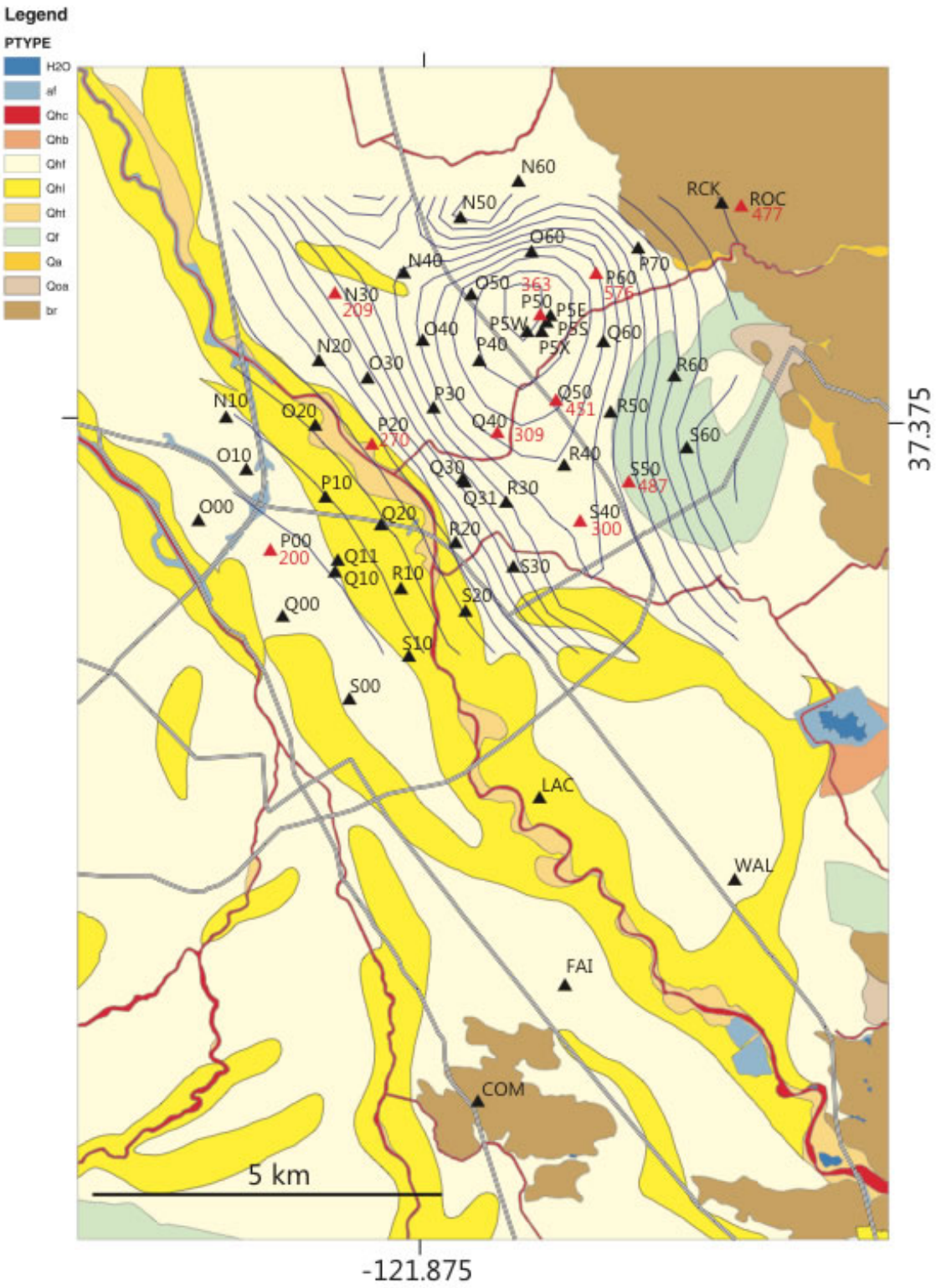
Legend
PTYPE
H2O
af
Qhc
Qhb
Qhf
Qhl
Qht
Qf
Qa
Qoa
br
N60
N50
RCK
ROC
477
O60
P70
N40
P60
576
O50
363
P50
P5E
N30
209
P5W
P5S
Q60
O40
P40
P5X
N20
O30
R60
P30
Q50
431
R50
N10
O20
P20
270
Q40
309
S60
O10
R40
S50
487
Q30
P10
Q31
R30
O00
Q20
S40
300
R20
P00
200
Q11
S30
Q10
R10
S20
Q00
S10
S00
LAC
WAL
FAI
COM
5 km
37.375
-121.875

Figure 2, new station locations in red and previous station locations in black

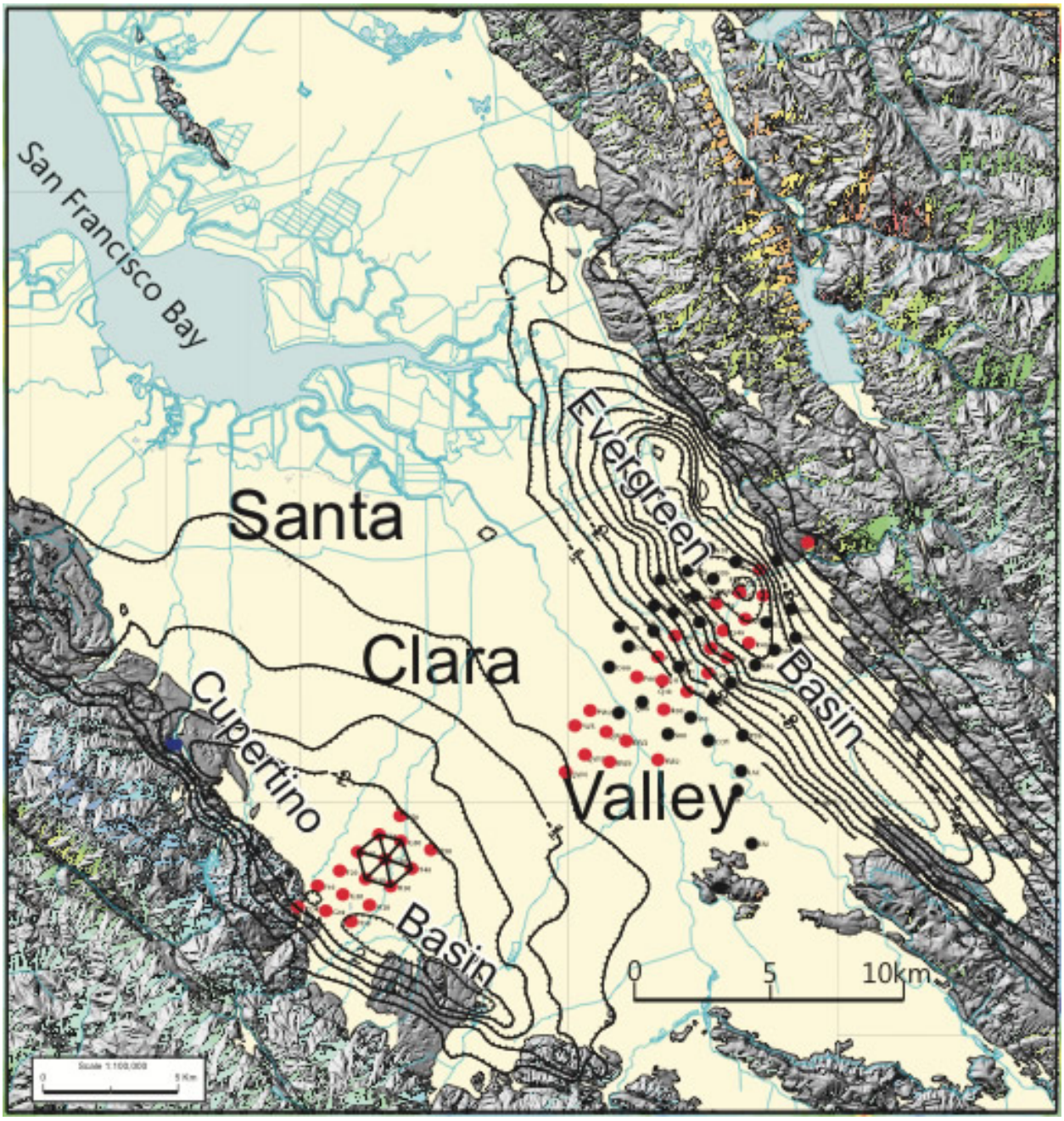

Figure 3

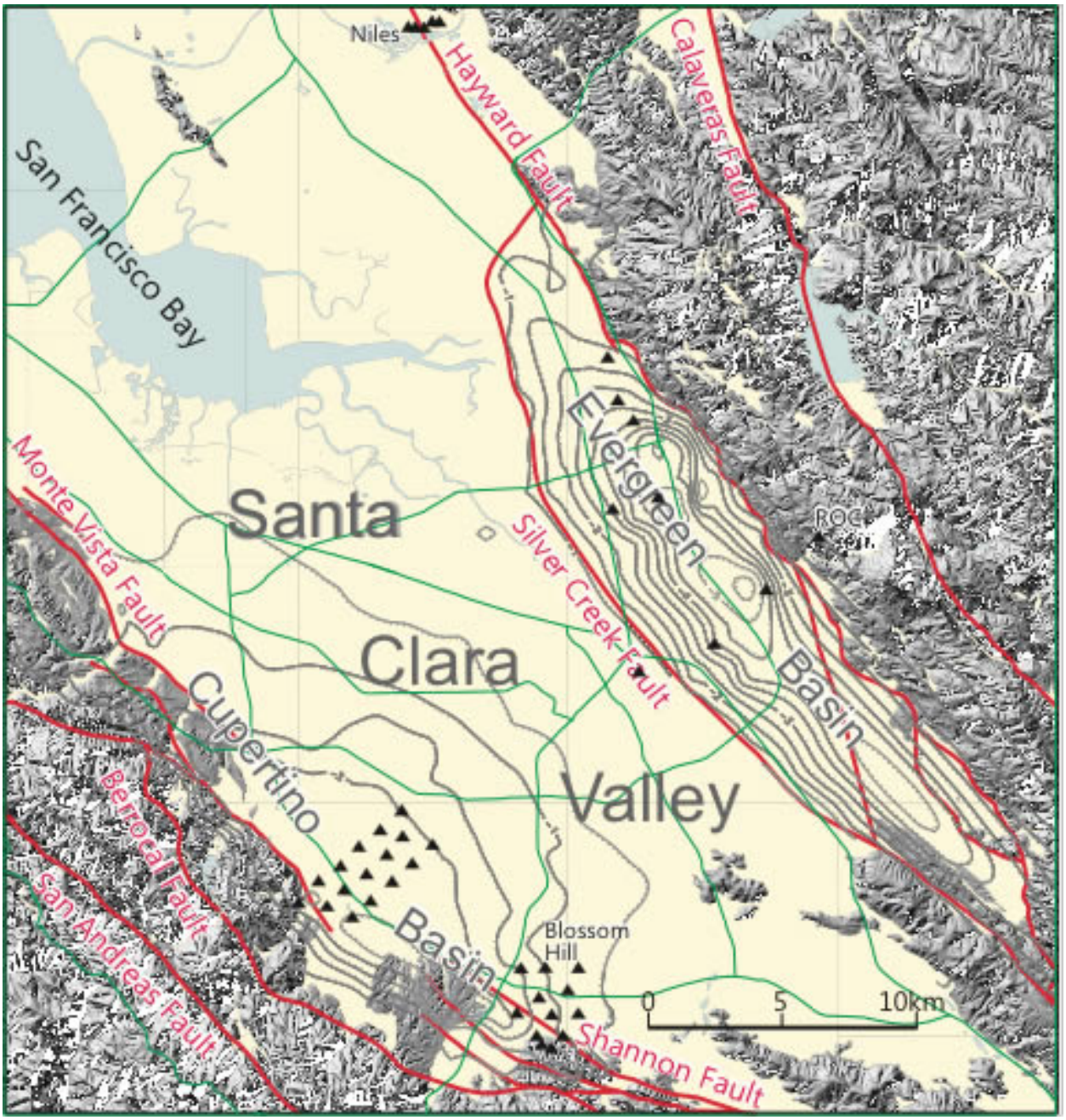
Niles
Hayward Fault
Calaveras Fault
San Francisco Bay
Evergreen
Santa
Clara
Valley
Basin
Silver Creek Fault
Monte Vista Fault
Cupertino
Berrocal Fault
San Andreas Fault
Basin
Blossom Hill
0
5
10km
Shannon Fault

Figure 4

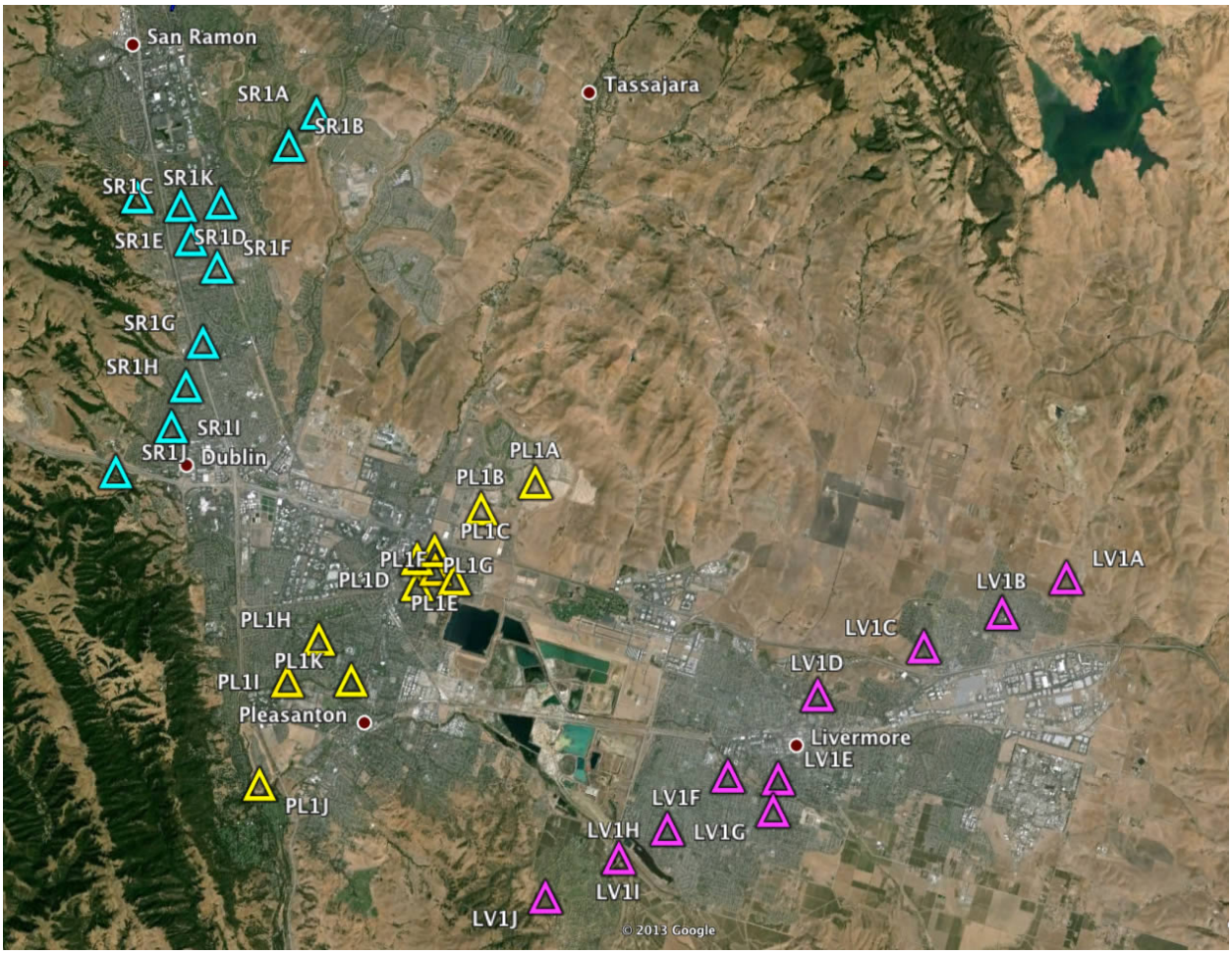
San Ramon
Tassajara
SR1A
SR1B
SR1C
SR1K
SR1E
SR1D
SR1F
SR1G
SR1H
SR1I
SR1J
Dublin
PL1A
PL1B
PL1C
PL1F
PL1G
PL1D
PL1E
PL1H
PL1K
PL1I
Pleasanton
PL1J
LV1A
LV1B
LV1C
LV1D
Livermore
LV1E
LV1F
LV1H
LV1G
LV1I
LV1J
© 2013 Google

Figure 5

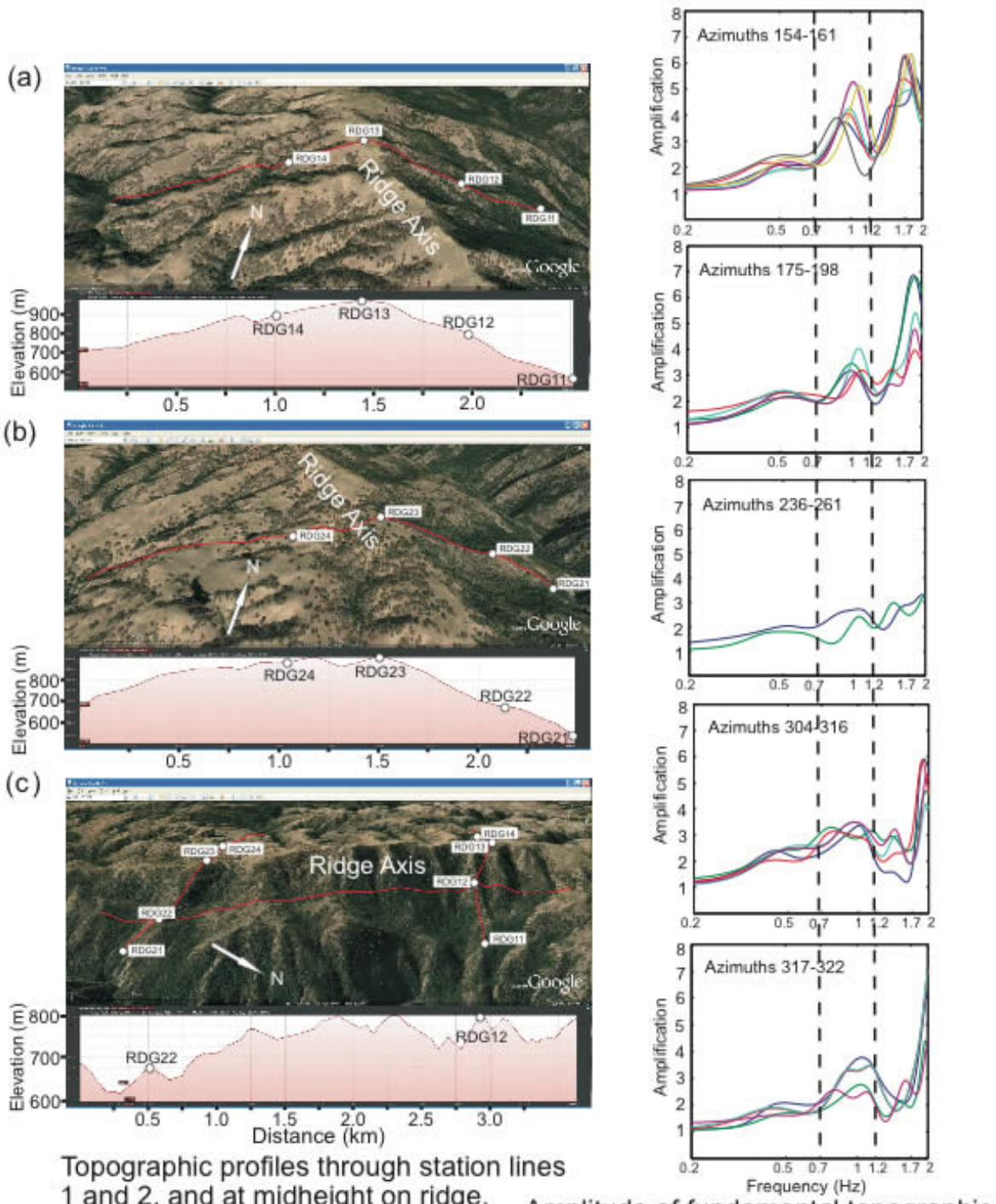

Topographic profiles through station lines 1 and 2, and at midheight on ridge.

Amplitude of fundamental topographic resonance peak near 1 hz as a function of source azimuth. Maximum along trend of axis of Poverty Ridge. Station RDG23.

Figure 6


Google Earth Pro
File Edit View Tools Add Help
44.627, -88.757
258 m
© 2012 Google
©2010 Google
lat 37.513725° lon -121.872478° elev 601 m
Eye alt 919 m
Graph: Min, Avg, Max Elevation: 546, 646, 768 m
Range Totals: Distance: 1.18 km Elev Gain/Loss: 219 m, -224 m Max Slope: 56.5%, -79.9% Avg Slope: 31.1%, -42.1%
768 m
725 m
700 m
675 m
650 m
625 m
600 m
575 m
546 m
552 m
15.0%
0 m
0.07 km
0.15 km
0.22 km
0.30 km
0.37 km
0.45 km
0.52 km
0.60 km
0.67 km
0.75 km
0.82 km
0.90 km
0.97 km
1.05 km
1.12 km
1.18 km

Figure 7

Figure 8

Figure 9

Figure 10